PHASE CHANGE IN MICROCHANNEL HEAT SINK UNDER FORCED CONVECTION BOILING

Linan Jiang[1], Man Wong[2], Yitshak Zohar[1]

[1]Department of Mechanical Engineering, [2]Department of Electrical and Electronic Engineering
The Hong Kong University of Science & Technology, Clear Water Bay, Kowloon, Hong Kong
Tel: 852 2358 7194, Fax: 852 2358 1543, Email: mezohar@ust.hk

ABSTRACT

A microchannel heat sink system, consisting of parallel microchannels, distributed temperature micro-sensors and a local heater, has been fabricated and characterized. V-grooves with hydraulic diameter of either 40μm or 80μm were formed by bulk silicon etching. The heater and temperature microsensor array were fabricated using surface micromachining. Microchannels were realized by bonding a glass wafer to the silicon substrate, resulting in a transparent cover for flow visualization. Phase change during the boiling process was studied under forced convection conditions, where DI water was used as the working fluid. No boiling plateau, associated with latent heat, has been observed in the boiling curves of microchannel heat sinks. Flow visualization was carried out to understand the boiling mechanism in such a system. Three phase-change modes were observed depending on the input power level. Local nucleation boiling within the microchannels occurred at low power level. At moderate levels, large bubbles developed at the inlet/outlet regions, and the upstream bubbles were forced through the channels and out of the system. At higher input power levels, a stable annular flow mode was observed, where a thin liquid film coated each channel wall until critical heat flux conditions developed with a dryout of the system.

INTRODUCTION

A number of MEMS devices are being designed based on the principle of liquid-to-vapor phase change, such as micro heat sinks [1], micro heat pipes [2] and micro heat pumps [3]. Therefore, the area of two-phase forced convection heat transfer in microchannels is a developing field with many engineering applications. As the field of microfluidics and micro heat transfer continues to grow, it becomes increasingly important to understand the mechanisms and fundamental issues involved with two-phase flows in micro geometries.

A few researchers have studies the boiling process in microchannels. However, all the studies up-to-date deal with channels with dimensions larger than 300μm. The lack of data for smaller dimensions signify the need for extensive research in this area. Zhukov and Yarmak [4] reported that boiling in channels with diameter of 800μm under heat pulse resulted in an abrupt pressure rise in the heated section which can cause the flow to stop quickly and, in some cases, may result in reverse flow. Peng and Wang [5] investigated the phase change in microchannels 600μm in width and 700μm in length. They observed fully developed nucleate boiling with no bubble growth inside the microchannels. Browers and Mudawar [6] reported that the production of vapor bubbles, in microchannels 500μm in diameter, enhanced the heat transfer rate and also increased the pressure drop.

Bubble activity of forced convection boiling in microchannels was also investigated. Klausner and Mei [7] developed a simple model for estimating the maximum and minimum cavity radius required for ebullition in two-phase flow with heat transfer. They demonstrated that the nucleation site density in flow boiling is correlated with the ratio of the maximum to minimum cavity radius. They suggested that complete suppression of nucleation sites occurred for a ratio between 50 and 150. James and Carl [8] observed very little, if any, bubbly flow in 1.88mm-high channels. Kandlikar *et al.* [9] concluded that the wall superheat has a major influence on the bubble growth rate. Peles *et al.* [10] conducted visualizations of forced convection boiling in microchannels with hydraulic diameter of 300μm. Pictures of individual bubbles as well as vapor-liquid interface within the channels were presented.

In a previous work [11], we studied the boiling process in microchannels, with hydraulic diameter of either 40μm or 80μm, by measuring the temperature distribution, liquid flow rate, and power dissipation for a variety of test conditions. No plateau was observed in the boiling curves for the microchannel heat sinks, different from results reported for macrochannel heat sinks. This was attributed to the restricted bubble formation and growth mechanisms due to the channel micro size, which can be verified only by flow visualizations. Therefore, in this work, transparent microchannel heat sinks have been fabricated to allow visualizations of the flow pattern with simultaneous measurements of the temperature field, liquid flow rate and input power during forced-convection boiling.

DEVICE DESIGN AND FABRICATION

The device was designed as an integrated micro-system consisting of either 34 or 35 microchannels, a localized heater and a 2-D array of temperature micro-sensors on a single die. The die size was 10mm×20mm. The micro heat sinks included an array of grooves, formed by bulk TMAH Si etch, either 50μm or 100μm in nominal width. A Pyrex 7740 glass wafer was anodically bonded to the silicon substrate to cover the grooves. The resulting transparent microchannels, with triangular cross-sections, allowed *in-situ* video recording of the flow field. The integrated heater and distributed temperature microsensors were fabricated on the silicon wafer using standard surface micromachining techniques.

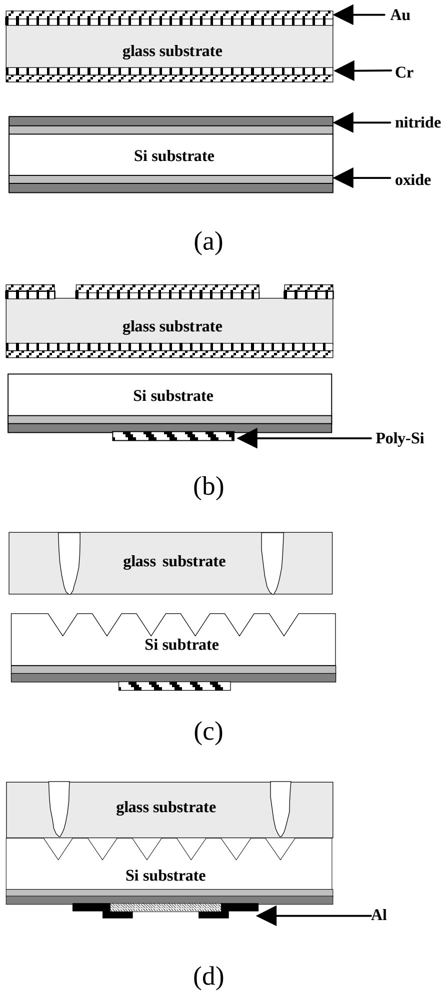

Figure 1: Schematic cross sections of the major fabrication steps.

Schematic cross sections of the major fabrication steps are shown in Figure 1. The starting substrates were a 100mm, (100) orientated, p-type silicon wafers having a thickness of 525μm and resistivity of about 17Ω·cm. The fabrication began with thermal growth of a 0.3μm oxide layer, followed by a 0.3μm LPCVD low stress silicon nitride at 840°C for insulation (Figure 1(a)). A 0.4μm polysilicon film was deposited on top of the nitride and patterned to serve as the heater and the sensor material (Figure 1(b)). The dumbbell-shaped thermistors were formed by selectively implanting phosphorus into an 8μm stretch of polysilicon in the center of the dumbbell [12]. The dosage was 5x10^{14}/cm^{2} and the implant energy was 60KeV. The remaining portions of the sensors and the serpentine-shaped heater were heavily doped with arsenic, 8×10^{15}/cm^{2}, to reduce the resistivity. The doped polysilicon was then annealed at 900°C for 30 minutes. The oxide layer on the wafer backside was patterned to serve as an etch mask. This was followed by bulk Si etch in a 25wt% aqueous TMAH solution at 85°C (Figure 1(c)), while the front side of the wafer was protected. After the oxide etch mask was stripped, a 1μm Al-Si layer was sputtered, patterned, and sintered at 450°C for 30 minutes to form the interconnects (Figure 1(d)). Meanwhile, a stack of 0.4μm Au layer on top of 0.04μm Cr thin film was sputtered on a Pyrex 7740 glass wafer to serve as an etch mask. After patterning holes for the channel inlet/outlet, the glass wafer was etched through in 40% HF, and followed by stripping the Cr/Au layers. The Si wafer and glass wafer were then aligned and pre-bonded together, immediately after a cleaning process, and were anodically bonded at 340^{o}C with applied voltage of 700V (Figure 1(d)).

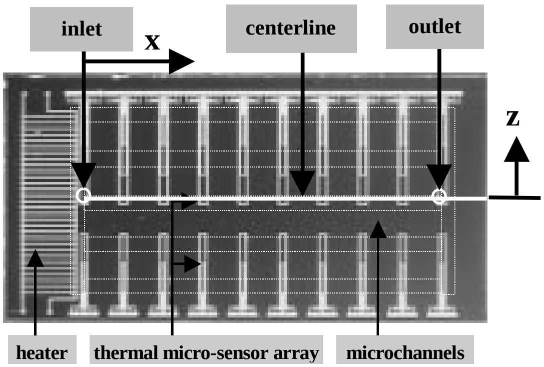

Figure 2: Device overview showing heater and temperature microsensor array.

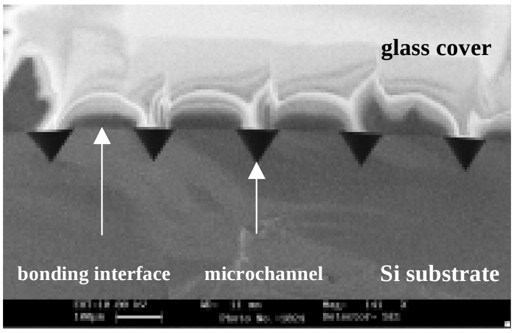

Figure 3: Cross-sectional SEM picture showing the triangular shape of the microchannels.

A plan-view picture of the fabricated device is shown in Figure 2, where the local heater and the temperature-sensor array are marked. The device cross-sectional SEM picture, shown in Figure 3, illustrates the triangular shape of the microchannels buried between the boded silicon and glass wafers.

EXPERIMENTAL SET-UP

The experimental set-up, shown schematically in Figure 4, consists of four sub-systems: (i) external fluid-handling system, (ii) micro-channel test chip, (iii) data acquisition system and (iv) video recording system. The external fluid-handling system includes a high-pressure gas source, a pressurized fluid reservoir, pressure gauges, valves, a filter, inlet/outlet adapters, a cold water container, and a volumetric graduate. A power source, a multimeter and a PC formed the data-acquisition system. The video recording system was basically a CCD camera mounted on a microscope and was connected to a videocassette recorder (VCR).

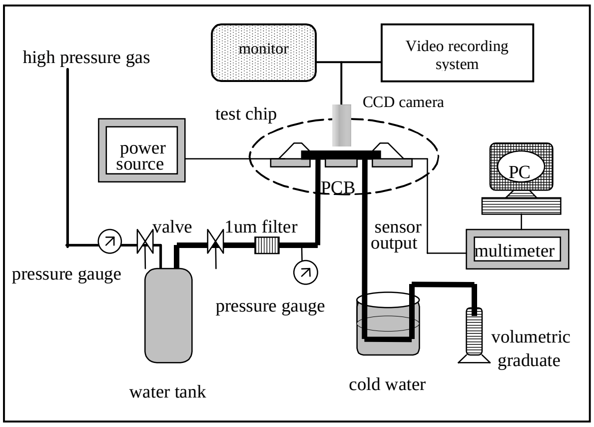

Figure 4: Experimental set-up.

The test chip was packaged on a printed circuit board (PCB) with a metal pattern designed for I/O connections for the heater and sensors. Ceramic adapters connecting the external system to the micro-channel array enabled the flow through the entire system without leakage. DI water was used as the working fluid in the forced-convection experiments. The water was supplied from a pressurized tank at room temperature, while the driving pressure was adjusted by a pressure regulator resulting in a controlled flow rate. Prior to entering the micro-channel heat sink, the water was passed through a 1μm filter in order to prevent channel plugging. The outlet tube was immersed in cold water to condense the exit fluid and allow volume flow-rate measurements using a graduate. The input power was controlled by adjusting the voltage applied to the heater, and the output of the sensors was collected for selected test conditions by the data acquisition system. The transparent glass ceiling of the channel allowed the recording of the phase-change pattern using the VCR.

RESULTS AND DISSCUTION

The measurements were conducted with DI water forced through the heat-sink inlet near the heater, as shown in Figure 2. The evolving phase-change pattern was recorded on a videotape for subsequent playback and analysis, while the flow rate, input power and temperature distribution were simultaneously recorded for a variety of test conditions.

Jiang *et al.* [11] speculated that the boiling plateau had not been observed due to the small size of the channels. In the experiments, the diamond-shaped microchannels were embedded in between two bonded silicon wafers. In this work, however, the triangular-shaped microchannels were embedded between silicon and glass wafers. Therefore, the boiling-curve measurements were first repeated, where the 2-D temperature field was recorded as a function of the input power, q, for different flow rates, Q_v. The spanwise temperature distributions along the z-axis were found to be uniform, consistent with the previous data [11]. Therefore, only the streamwise temperature distributions along the device centerline, $T(x; z=0)$, are reported here. A typical set of data, for water flow rate of 2mL/min, is shown in Figure 5. The temperature distributions are fairly uniform for all input-power levels, except for the sensor nearest to the heater. At the lower input power, 5.1watt, the flow was in single-liquid phase throughout the channels. Increasing the power above 11.4watt resulted in two-phase flow within the channels. The fraction of vapor increased with the input power until critical heat flux (CHF) conditions developed at 29.9watt, when the exit flow quality was one as the channel flow was in single-vapor phase.

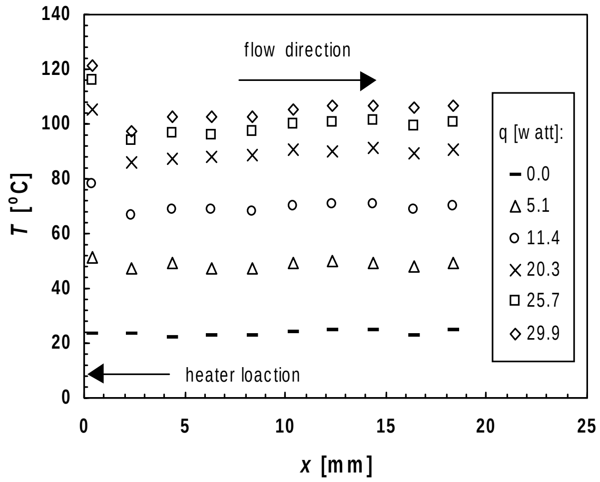

Figure 5: Device temperature distributions along the microdevice (Q_v=2mL/min, 50μm width, 35 channels).

The average temperature along the device centerline was used to construct the boiling curves summarized in Figure 6 for four different test conditions. All the curves collapse together if the device temperature and the input power are normalized by their respective values at CHF conditions, i.e. T_{CHF} and q_{CHF}; T_0 is the reference room temperature. Although the curves are not linear, the temperature increases monotonically with the input power. No boiling plateau, schematically shown at the inset in Figure 6, can be observed as reported earlier [11]. The slope gradually decreases until CHF conditions develop, after which the device temperature increases sharply. Three flow regimes are marked in Figure 6 based on the phase-change modes detected during the subsequent flow visualizations.

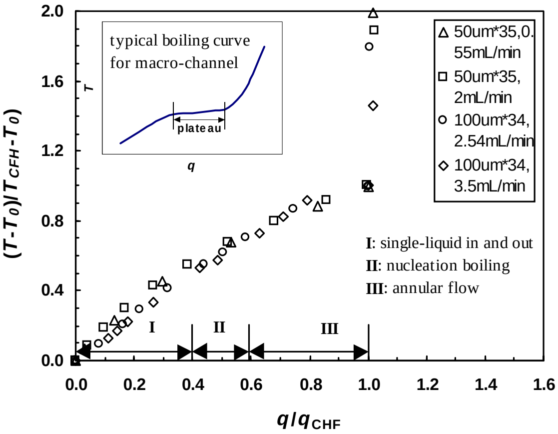

Figure 6: Boiling curves for microchannel heat sinks.

The boiling plateau, observed in macrochannel flows, is associated with the latent heat required to change the fluid phase from liquid to vapor. It was suggested that the boiling process in microchannels could be affected due to the channel microsize by restricting the bubble formation and growth mechanism. Consequently, flow visualization experiments were conducted to understand the phase-change evolution inside the microchannels with increasing input power. For low input power, $q/q_{CHF}<0.4$ (zone I), the flow in and out of the device was in single-liquid phase corresponding to the linear increase of the temperature with the input power. Clearly, almost all the increased power dissipation is transferred into the liquid, linearly increasing its internal energy, i.e. its temperature.

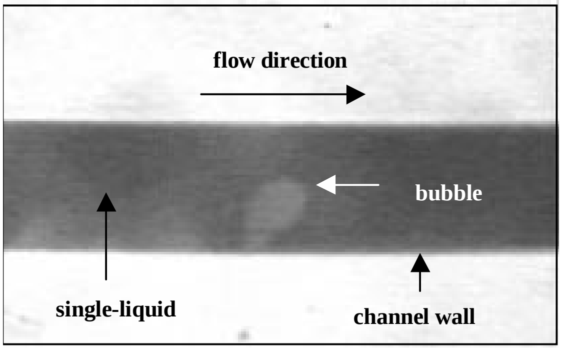

Figure 7: Nucleate boiling mode inside the micro-channel (q/q_{CHF}=0.4, 50µm width, 35 channels).

The first observed mode of phase change, local nucleation boiling, was already detected at this low input-power range. Bubbles could be seen forming at some locations along the channel walls at a few active nucleation sites. The bubble formation, growth and explosion could be seen clearly inside the micro-channel, as demonstrated in Figure 7, at a fairly high frequency. However, there were very little, if any, active nucleation sites along the channel walls. Furthermore, most of the nucleation sites became inactive after one or two runs suggesting that they probably were residues of the fabrication process. Consequently, this local nucleation-boiling mode has negligible effect on the boiling curve, which sustains its linearity in the low input power range.

At moderate input-power levels, $0.4<q/q_{CHF}<0.6$, large bubbles were generated at the inlet/outlet common passages, as shown in Figures 8(a) and 8(b), which connect the microchannels to the device common inlet/outlet. The boiling activity at these larger passages became stronger with increasing input power. As a result, the boiling-curve slope in zone II is smaller than the slope in zone I since the bubble-formation process (phase change) consumed some of the input power.

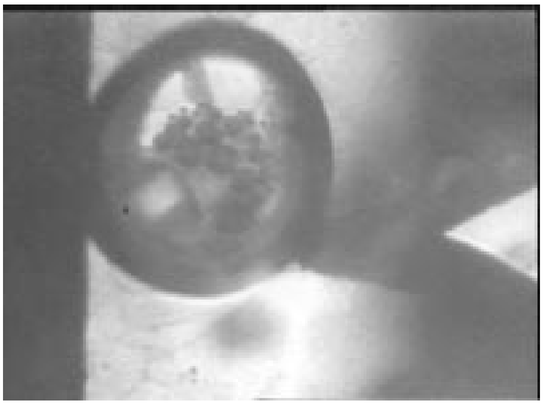

Figure 8(a): Bubble forms and grows at inlet manifold (q/q_{CHF}=0.4, 50µm width, 35 channels).

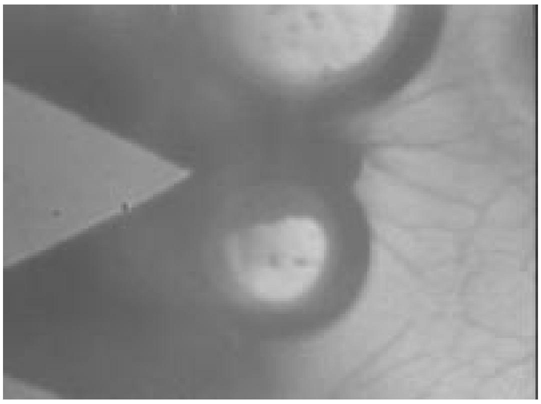

Figure 8(b): Bubble forms and grows at outlet manifold (q/q_{CHF}=0.4, 50µm width, 35 channels).

Furthermore, most of the upstream bubbles were forced through the channels as a slug flow, as demonstrated in Figure 9. The bubbles typically grew to a size larger than the microchannel dimensions. Therefore, these bubbles blocked the channel entrance, as shown in Figure 9(a), until the upstream pressure was high enough to force them into the microchannel. In some cases, the bubbles traveled slowly along the channel as slug flow shown in Figure 9(b). In most instances, however, the bubbles were ejected at high speed through the microchannel and could not be detected until they re-appeared at the channel exit as shown in Figure 9(c).

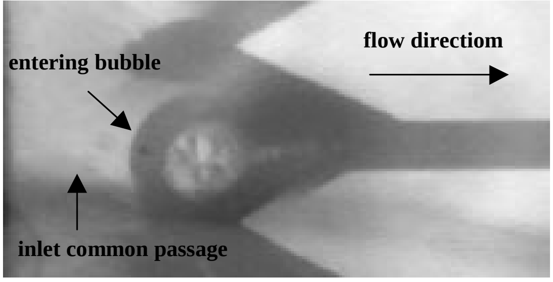

Figure 9(a): Bubble entering the micochannel (q/q_{CHF}=0.5, 50μm width, 35 channels).

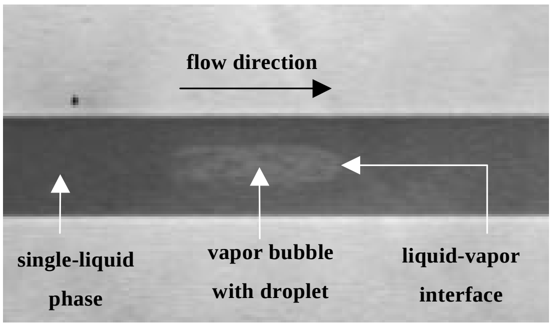

Figure 9(b): An example of an upstream bubble forced through the microchannel as a slug flow patter (q/q_{CHF}=0.5, 50μm width, 35 channels).

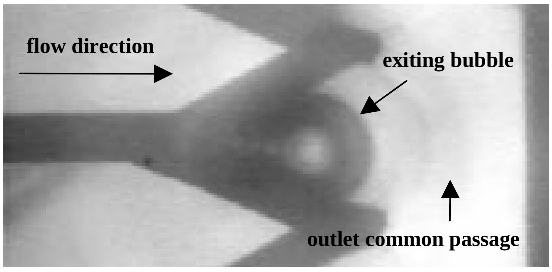

Figure 9(c): Bubble exiting the microchannel (q/q_{CHF}=0.5, 50μm width, 35 channels).

At a power level of about q/q_{CHF}=0.6, between zone II and zone III, an annular flow mode was observed with liquid droplets within the vapor core, as shown in Figure 10, and the vapor-liquid interface in the channel appeared to be quite random. This mode seemed to be an unstable, transition stage, since it was not always detected and short lived whenever it did appear. However, the nucleation sites on the walls were completely suppressed and bubble formation inside the channels could no longer be observed. Most likely this resulted from the activity of the upstream bubbles as they passed through the microchannels.

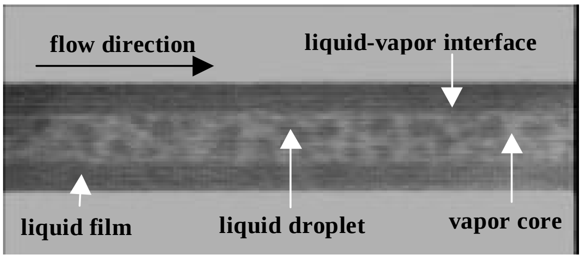

Figure 10: Unstable annular flow with liquid droplet in the vapor core (q/q_{CHF}=0.6, 50μm width, 35 channels).

With the increase of the input power level to a higher range, 0.6<q/q_{CHF}<0.9, a stable annular flow mode shown in Figure 11 was developed. A thin liquid film coated each channel wall, and an interface between the liquid film and the vapor core was clearly distinguishable. No liquid droplets existed within the vapor core, indicating that the vapor-core temperature was higher than the liquid saturation temperature. At this power range, zone III, evaporation at the liquid film-vapor core interface dominated the heat transfer from the channel wall to the fluid. Since the heat is conducted through the liquid film to the interface, the temperature at the wall has to increase to allow higher heat transfer rate required by the increased input power. The temperature would increase linearly with the input power if the film thickness stays constant. However, the film thickness decreased with increased power, due to the evaporation process, resulting in higher quality of the two-phase exit flow. Thus, the temperature increased slightly with decreasing slope as the input power increased.

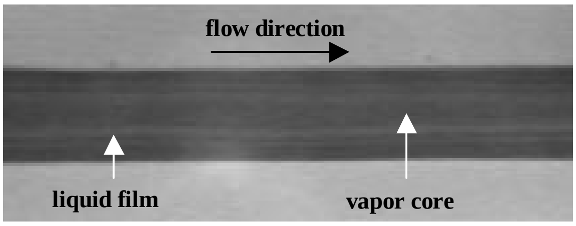

Figure 11: Stable annular flow mode in the microchannel (q/q_{CHF}=0.8, 50μm width, 35 channels).

As the input power approached the critical heat flux level, $q/q_{CHF}\rightarrow 1$, the liquid film started to dry out at certain portions on the wall, primarily at the channel entrance and exit regions, as shown in Figures 12(a) and 12(b) respectively. Once the dry out process had been triggered, it proceeded rapidly such that the entire liquid in the channels was completely vaporized. This was accompanied by a sharp rise in the device temperature, often melting the soldering material of the wirebonds. Consequently, it was impossible to continue the measurements once the CHF conditions had developed.

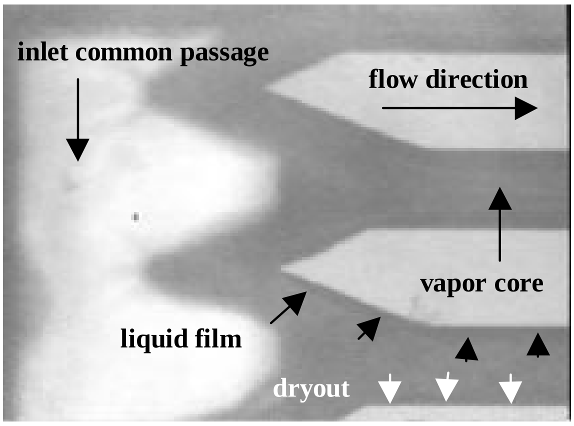

Figure 12(a): Flow pattern at the inlet near CHF conditions (q/q_{CHF}=0.9, 100μm width, 34 channels).

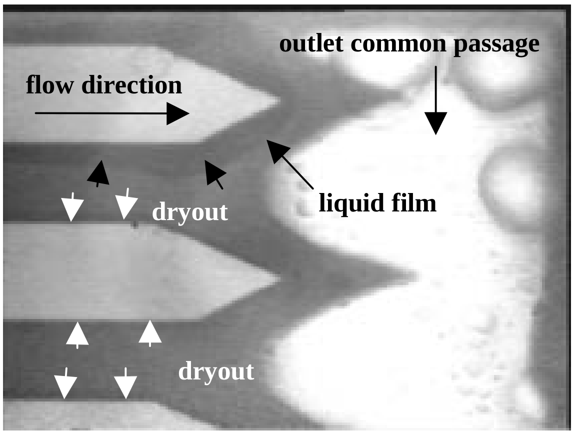

Figure 12(b): Flow pattern at the outlet near CHF conditions (q/q_{CHF}=0.9, 100μm width, 34 channels).

CONCLUSIONS

A transparent microchannel heat sink system was designed and fabricated with a localized heater and an integrated temperature sensor array. The device allowed simultaneous qualitative visualization of the flow pattern and quantitative measurements of the 2-D temperature distribution, water flow rate and heat flux, during forced convection boiling experiments. At lower input power range, local nucleation boiling was observed, where bubbles could form, grow and explode even in such microchannels with hydraulic diameter of about 40μm. However, nucleation sites along the channel were very rare, especially after the fabrication residues had been cleaned up in the first run. At intermediate power level, slug flow developed as upstream bubbles, generated at the inlet common passage, were forced through the channels completely suppressing what was left of the active nucleation sites. At a higher input power range, stable annular flow mode was developed, with clear liquid film-vapor interface but no liquid droplets in the vapor core.

Due to the microscale size of the channels, a stable vapor core is established at an early stage, such that evaporation at liquid film-vapor core interface becomes the dominant heat-transfer mechanism over a wide range of the phase-change process. Thus, the typical bubble generation and growth mechanisms commonly observed in forced-convection boiling in macrochannels are suppressed. This boiling process, which leads to the plateau in the boiling curve, cannot develop in microchannels. Consequently, no plateau is observed in the boiling curves of such microchannel where the temperature increases monotonically with the input power though with decreasing slope.

ACKNOWLEDGMENTS

The work was supported by the Hong Kong Research Grant Council through RGC grant HKUST579/94E.

REFERENCES

[1] Tuckerman, D. B. & Pease, R. F. W., *IEEE Electron Device Lett,* EDL-2, p.126, 1981.

[2] Peterson, G.P., *Appl. Mech. Rev.*, 45, pp. 175-189, 1992.

[3] Drost, M.K., Beckette, M.R., and R.S. Wegeng, *Microscale heat transfer, ASME,* HTD-Vol.291, pp. 35-43, 1994.

[4] Zhukov, V.M. and Yarmak I.L., *Cryogenics*, 30, pp. 282-286, 1990.

[5] Peng, X.F., Wang, B.X., *Int. J. heat Mass Transfer,* 36, pp. 3421-3427, 1993.

[6] Bowers, M.B. & Mudawar, I, *Int. J. Heat Mass Transfer*, 37, pp. 321-332, 1994.

[7] Klausner J.F. and Mei R., *proceedings of convective flow boiling*, John C. Chen, Editor, Talor & Francis, pp. 155-160, 1995.

[8] James E.O. and Carl M.S., HTD-Vol.273, *Fundamentals of Phase Change: Boiling and Condensation, ASME,* pp. 81-91,1994.

[9] Kandlikar S.G., Mizo V., Cartwright M. and Lkenze E., HTD-Vol.342, *National Heat Transfer Conference*, *ASME*, pp. 11-18, 1997.

[10] Peles, Y.P., Yarin L.P. and Hetsroni G., submitted to *J. Milti-phase Flow*, 1999.

[11] Jiang, L., Wong, M. and Zohar, Y., *J. Microelectromech. Syst.*, 8, 1999, in print.

[12] Jiang L., Wong M. and Zohar Y., *Measurement Science and Technology,* 10, pp. 653-664, 1999.